Multispectral Analysis of Miniature Nuragic Bronze Flasks

Carlo Nocco [1], Francesca Assunta Pisu [2], Daniele Chiriu [2], Anna Depalmas [3],
Sergio Augusto Barcellos Lins [4,*] and Antonio Brunetti [5]

[1] Dipartimento di Storia, Scienze Dell'uomo e Della Formazione, Università di Sassari, 07100 Sassari, Italy; c.nocco3@studenti.uniss.it

[2] Department of Physics, Università di Cagliari, Cittadella Universitaria, 09042 Monserrato, Italy; francescaassunta.pisu@dsf.unica.it (F.A.P.); daniele.chiriu@dsf.unica.it (D.C.)

[3] Dipartimento di Scienze Umanistiche e Sociali, Università di Sassari, 07100 Sassari, Italy; depalmas@uniss.it

[4] Dipartimento di Scienze di Base e Applicate per L'ingegneria, Università Degli Studi di Roma "La Sapienza", 00161 Rome, Italy

[5] Dipartimento di Chimica e Farmacia, Università di Sassari, 07100 Sassari, Italy; brunetti@uniss.it

* Correspondence: sergio.lins@roma3.infn.it

Abstract: Miniaturized bronze flasks represent a small portion of a wide metallurgical production that flourished in Sardinia (Italy) between the Final Bronze Age (FBA) and the Early Iron Age (EIA). They replicate a well-known and symbolic type of object, the pilgrims' flask, common in all Europe and Mediterranean basin, and have but few archaeological parallels. For these reasons, their characterization can be considered important from an archaeological perspective. Three flasks, preserved at the *Antiquarium Arborense* museum (Oristano), were analyzed by X-Ray Fluorescence Spectroscopy (XRF) and Raman spectroscopy, integrated by multispectral images. The samples, coming from illegal excavations, posed two problems: establishing their authenticity and investigating the alloy composition of such particular objects. All specimens presented a widespread degradation in the outer surface: XRF and Raman spectroscopy indicated the presence of copper oxides, calcium and copper carbonates deposits. The abscence of Zn, a clear marker of forgeries, was not detected by XRF. In two of the flasks, an unusual Sn content above 20%, was detected. For FBA and EIA, especially regarding southern Europe, Sn was extremely rare, and was possibly used with caution. Further results are presented herein.

Keywords: Sardinia; miniature bronze objects; pilgrim flask; XRF; Monte Carlo; Raman

1. Introduction

In the period between the Final Bronze Age and Early Iron Age in Sardinia, the Nuragic civilization was responsible for a large and diverse metallurgical production, mostly with bronze [1]. Bronze flask pendants are miniaturistic reproductions of similar Early Iron Age ceramic vessels [2–5] that replicate the basic characteristics of the pilgrim flask' prototype: they have a flat-convex body with a truncated cone shape decorated with concentric grooves, four handles, and a long cylindrical neck surrounded by stylized straps that end with an original ring of suspension.

Nineteen (19) miniature bronze flasks have been found in Sardinia and the Italian peninsula (Figure 1): one from an unknown site [4], one from *Nughedu San Nicolò* [2,3,6], one from *Borore* [2,3], two from the *nuraghe Nurdòle-Orani* [2,3], two from the sacred well of *Su Tempiesu-Orune* [2,3,7], one from the sanctuary of *Su Monte-Sorradile* [4], one from *Mont'e Prama-Cabras* [8], and four from the territory of Sinis [9], but without a proper archaeological context. The remaning six flasks come from the Etruscan necropolis of Montaione [10], San Cerbone-Populonia [10] and Vetulonia [10]. The flasks from Sinis area (Figure 2) [9], recovered during a police operation in 1992, are currently preserved in Oristano (Sardinia), at the museum *Antiquarium Arborense*.
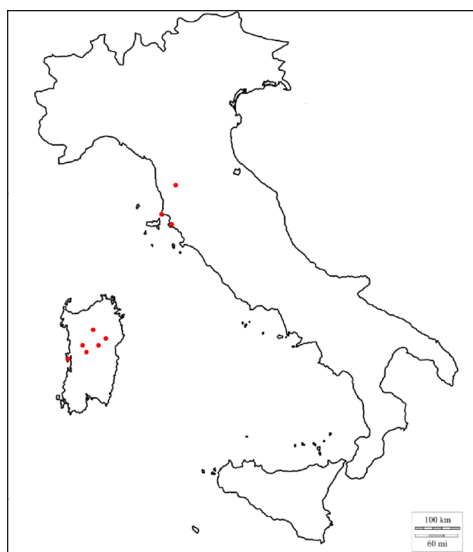
Figure 1. Distribution map of bronze nuragic flasks in Sardinia and the Italian peninsula.
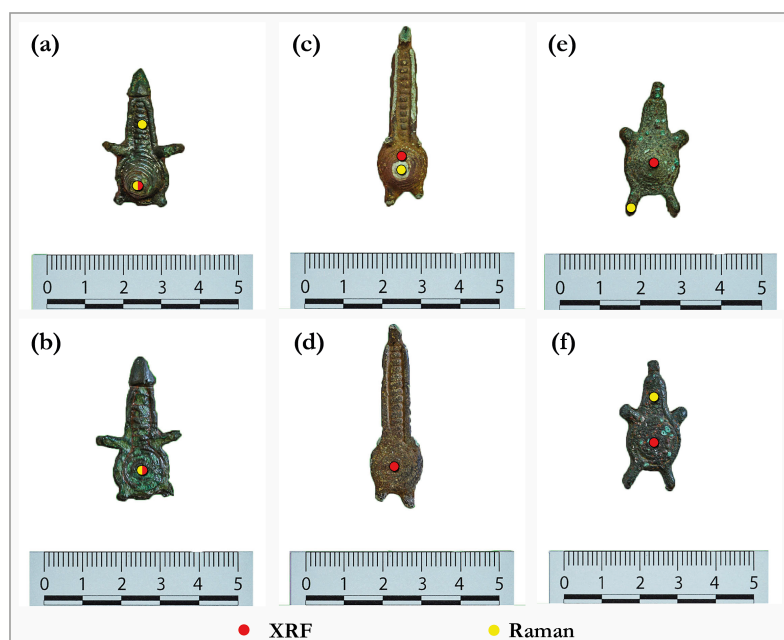
Figure 2. The front and back side of miniature flasks: #1 (**a**,**b**), #2 (**c**,**d**), #3 (**e**,**f**). Red dots indicate the spots where XRF spectra were collected, while the yellow dots indicate those where Raman spectra were collected.

Due to the relative rarity of these miniature bronze flasks, many questions remain open. First, their use and importance within the Nuragic civilization and, second, their authenticity. Three of the four flasks thought to belong to the Sinis region were investigated in this work. It is not uncommon that forgeries are inserted among authentic lots [11], so an authenticity check is almost always mandatory. Furthermore, they lack a proper archaeological context and were obtained possibily through illegal excavations. The flasks were retrieved by the police and their authenticity and/or site of origin is unknown.

These flasks are the first and only miniature pilgrim bronze flasks to be analyzed with multispectral techniques. Their bulk material chemical composition, representing the alloy originally used for the artifact manufacture, was obtained with X-Ray fluorescence (XRF) analyses coupled with a Monte Carlo algorithm (XRMC) capable of simulating X-rays interactions with matter [12,13].

The corrosion products, deposited in the objects' surface through the course of time, were investigated with Raman spectroscopy and with the XRF-XRMC method. The patina can be used as an indicative of the object's originality, as millenia-old corrosion layers are very hard to replicate artifically [14]. Furthermore, the patina can also provide information regarding the depositional conditions of the artefact [15].

2. Materials

- The miniature flask #1 (lenght 3.60 cm, width 2.20 cm, weight 13.02 g) is the one that is best preserved, possibly due to depositional conditions and/or a better post-depositional care. It's surface presents a vivid green color, clearly treated with paraloid. The upper part, where a suspension ring is missing, and the lower loops are deteriorated.
- Flask #2 (lenght 4.60 cm, width 1.10 cm, weight 14.46 g) does not differ morphologically from the previous one, but has much more pronounced wear on the surface, perhaps related to post-depositional phenomena, with loss of large portions of the loops and a general deterioration of the edges. Flasks #1 and #2 are similar to those from *Vetulonia-Poggio del Bello* [2,3] and those found at *Su Tempiesu-Orune* and *Nurdòle-Orani* (Sardinia). This flasks presents an orange surface. The central relief and parts of the neck are worn and present a light green color. It misses the lopps, stilyzed straps and the suspension ring.
- Flask #3 (length 3.40 cm, width 1.70 cm, weight 14.54 g) has, compared to the other samples, a shorter neck. It is comparable with the flask found in *San Cerbone-Populonia*. This flask presents a dark green color and is apparently less corroded in respect to the other previous flasks. The loops are preserved, but is misses the suspension ring.

3. Methodology

X-ray fluorescence analysis (XRF) is a well-known and non-destructive technique frequently used in archaeometry [16]. It is portable and capable of determining the chemical composition of the sample under investigation. Due to the penetrative nature of X-rays, the results obtained with XRF alone when investigating corroded artefacts, reflect the composition of the outermost layer instead of the bulk [17,18]. To overcome this problem, we made use of a Monte Carlo algorithm capable of simulating X-rays interaction with matter. This is achieved by simulating the experimental parameters (tube profile, setup geometry, etc.) and the sample itself (layers and composition). In this way, the sample parameters can be used to determine, with a quality superior to that obtained with XRF measurements, the real composition of the sample bulk, as well as determining the layers and their spatial distribution [13]. An initial guess of the patina layer composition was obtained with Raman spectroscopy.

3.1. X-Ray Fluorescence

The XRF experimental system used is composed of an X-ray tube (Amptek's Mini-X, Ag anode) operating at 40 keV, 5–20 µA and one X-123 SDD detector (also from Amptek). The unfiltered X-ray spectrum was collimated to 1 mm diameter, while no detector collimation was applied. Each measurement took approximately 60 s. Several spectra were collected at different spots, to assure repeatability.

3.2. Raman Spectroscopy

Near-Infrared (NIR) micro Raman scattering measurements were carried out in backscattering geometry with the 1064 nm line of an Nd:YAG laser. Measurements were performed under standard temperature and pressure conditions (STP) with a compact spectrometer (B&W TEK, Newark, NJ, USA) i-Raman Ex integrated system with a spectral resolution of less than 8 cm^{-1}.

The spectra were collected with different acquisition times, between 20 and 80 s, and power excitations between 20 and 30 mW concentrated in a spot of 0.3 mm^2 of the surface

through the BAC151B Raman Video Micro-Sampling System. A 20× Olympus objective was used to select the analysis spots.

3.3. XRMC Simulations

First, the XRF system response has to be fully characterized. This includes a precise digital reproduction of the system geometry and the X-ray detector response. Then, fluorescence peaks detected in the spectrum under simulation are used to build a guess model of the sample. The sample layers are first modelled according to an initial guess, prior the iterations that follow. The patina/corrosion layer composition and the protective layer (if any) parameters are initialized according to the Raman spectroscopy outputs and a careful visual inspection.

Following the creation of the initial sample model, a simulation is performed. The measured and simulated spectra are compared. The sample model is updated iteratively after each simulation, until it returns a perfect reproduction of the experimental XRF spectrum. When this is obtained, the simulated model, both in composition and structure, can be considered a faithful reproduction of the real sample.

This approach has shown a superior performance when compared to the more traditional approaches, based on background extraction and peak fitting, such as the Fundamental Parameter Method [19–22]. The Monte Carlo code used here is XRMC [12,23,24]. It is specialized for any type of X-Ray interaction with matter up to 100 keV of energy, well above the typical energies used in XRF. It is based on a continuously updated atomic database called xraylib [25]. This Monte Carlo code is fast, allowing one to obtain a good quality simulation, comparable to that from the real XRF experiments, in a handful of minutes, even on a laptop computer. XRMC performance is reported in [13], together with a minute description of its applications for Cultural Heritage materials.

Finally, the flasks investigated were modelled as a two or three-layered structure of infinite parallel planes accordingly. The modelled layers were: the protective film (if present), the patina/corrosion layer, and, lastly, the bulk, i.e., the alloy. The corrosion layer can be sub-divided into two or more layers, according to the modelled sample, as corrosion strata of ancient bronzes can present multiple complex layers [26,27]. The Monte Carlo code was executed on a laptop (Intel® Core i7). Each simulation took approximately 4 min.

4. Results

Flask #1, covered with a protective thin Paraloid-like (40 μm thick) layer, presented an unusually high value of Sn concentration within its matrix (40.3% wt), (see Table 1, Figure 3A), while the single-stratum patina (50 μm thick) has shown the presence chlorine and of several oxides through the detection of elements such as copper (14% wt), Sn (9.7% wt), As (0.3% wt) and Fe (0.3% wt). The Raman spectra of this sample (Figure 4A–C) shows a very broad peak around 440–530 cm^{-1} and a weak signal at 620 cm^{-1}. They confirm the presence of malachite $CuCO_3(OH)_2$, which has a maximum at 435 cm^{-1}, assigned to the translations of (Cu, CO_3) [28–30], and the presence of defective Cu_2O [30], having the two characteristic bands located at 520 and 625 cm^{-1}, assigned to Cu–OH and Cu–O vibration, respectively [31,32]. A very strong band at 296 cm^{-1} and a shoulder around 340 cm^{-1} are ascribed to tenorite [29,33], respectively to Ag and Bg mode of CuO. lastly, the wide band around 785 cm^{-1} can be ascribed to Cu-nitrate [34].
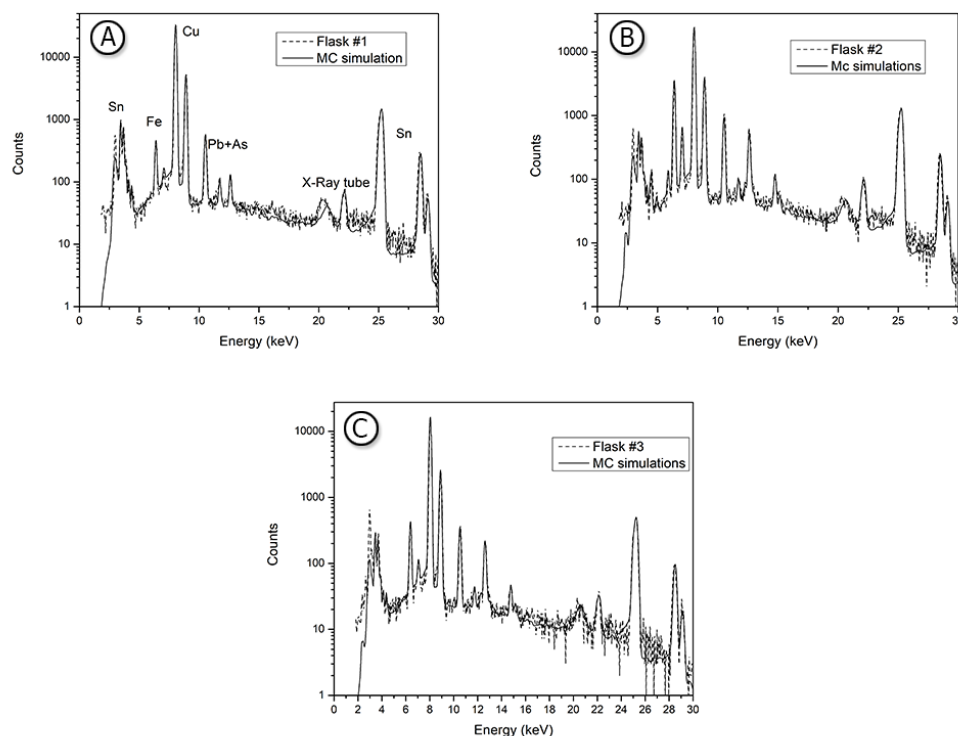
Figure 3. Experimental and simulated XRF spectra of front-back side of flasks: (**A**) #1; (**B**) #2 and (**C**) #3.

Miniature flask #2 (Table 1, Figure 3B) is formed by three layers as well: the protective film (70 μm thick), the patina-corrosion—also made of a single-statrum—(100 μm thick), and bulk. The bulk is clearly a Cu-Sn alloy. Copper weight concentration (38.1% wt) is lower than the that found within the other flasks bulk material; Sn, on the other hand, has a higher concentration (55% wt). The patina presented Cu (16% wt), Sn (8.5% wt), Fe (2.7% wt), Pb and As (both 0.6% wt). This phenomenon represents a bronze corrosion of Type I, as described in [35,36]. The Raman spectra (Figure 5) shows peaks around 440, 520, 625 cm^{-1}, which confirm the presence of malachite and defective cuprite. A strong peak around 986 cm^{-1} (region of $[SO4]^{2-}$ symmetric stretch) can be attributed to a copper sulfate phase like langite or brochantite [31]. The presence of sulfur is confirmed by XRF. Traces of amorphous carbon with typical shoulders approximately around 1340 and 1590 cm^{-1}, D and G bands [37], are detected.

Table 1. XRF: Compositional values of the matrix of flasks (wt %).

| Flask	Chemical Element (wt %)				
Bulk	Fe	Cu	Ag	Pb	Sn
#1	–	59	0.2	0.9	40.3
#2	–	38.1	1.0	7.5	55.0
#3	–	58.6	0.5	7.5	35.0
Patina					
#1	0.3	14	0.3	–	9.7
#2	2.7	16	0.6	0.6	8.5
#3	0.6	22	0.25	0.25	9
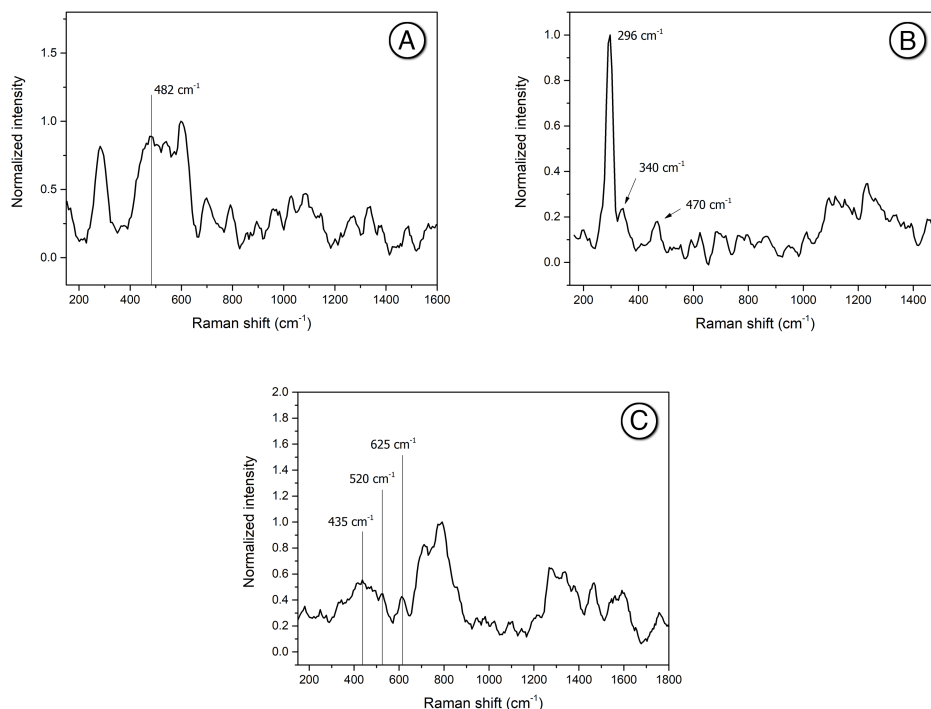
Figure 4. Flask #1: Raman spectra. (**A**) neck, green zone; (**B**) center back (**C**) cone top.
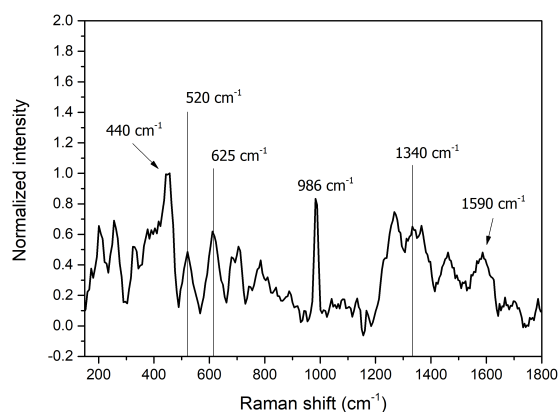
Figure 5. Flask #2: Raman spectrum of the front center.

Flask #3 model was also formed by three layers, with a single-stratum corrosion layer: the protective film (70 μm thick), the corrosion layer (100 μm thick), and bulk. Flask #3 XRF spectra (Table 1, Figure 3C) shows, for the matrix, a Cu content of 58.6% wt and a high Sn content (35% wt) Its composition is similar to that of flask #1. The patina layer presented Cu (22% wt), Sn (9% wt), As (0.25% wt), Pb (0.6% wt), and Fe (0.6% wt). Low concentrations of Cl (1.0–1.5% wt) and S were detected within the patina as well. From the Raman spectra, a strong peak at 800 cm^{-1} (Figure 6A), attributed to AsO$_4$ ions symmetric stretching mode, as in mimetite Pb5(AsO$_4$)$_3$Cl [29], was detected. Analogously to the other two samples, the presence of malachite and copper oxide was detected. In addition, a very strong signal of carbon (Figure 6B), with peaks position at 1320 and 1590 cm^{-1}, has been detected. The very strong carbon doublet arises from the degradation of organic residues (wax, oil, dust) used for maintenance [29], due to environmental pollution, or maybe the deposition of ashes.
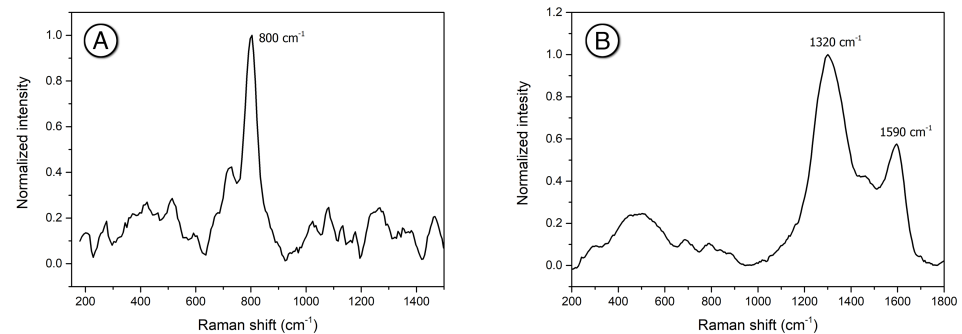
Figure 6. Flask #3: Raman spectra. (**A**) front left handle and (**B**) back neck center.

5. Discussion and Conclusions

Three miniature bronze models of pilgrim flasks have been analyzed. Their composition turned to be essentially a binary Cu-Sn alloy for flask #1 and a ternary Cu-Pb-Sn for the remaining two. No zinc was detected, scoring in favor of the miniatures' authenticity, and addressing the first research question. All flasks presented a very high weight percentage of Sn in their alloy composition. The possibility of tinning was dismissed as the models made with a thin tin-rich layer on top of the bulk resulted in mismatching spectra.

Tin was a relatively rare and precious metal in Sardinia and the south of Europe during the LBA and EIA, being most of it imported from outside the island. The excessive amount of Sn detected is surely intentional and possibily with a specific objective/application in mind. One of its most common use in metalsmithing is to strenghten the material, confering it more tensile strength. However, such quantities of Sn would make the metal more difficult to work instead [27]. Furthermore, it seems unreasonable to spend so much precious material to improve the mechanical properties of an object unlike to benefit from such improvements.

The more credible explication, is related to the nature of the objects themselves, i.e., being a pilgrim flasks' reproduction, and possibly a votive or otherwise iconic object that could be worn. The addition of Sn changes the final product colour, turning it more silver-like as Sn content increases [27,38]. Combined with the inherit value of the metal, Sn can render the object more "precious", from a votive perspective as well. These results are entirely new and fuel a new interpretation of such objects. Future works will aim in increasing the number of miniature pilgrim flasks examined to confirm this preliminary hypothesis.

Conflicts of Interest: The authors declare no conflict of interest.

References

1. Depalmas, A.; Melis, R.T. *The Nuragic People: Their Settlements, Economic Activities and Use of the Land, Sardinia, Italy*; Springer: Berlin, Germany, 2010; pp. 167–186.
2. Lo Schiavo, F. *Forme di Contenitori di Bronzo e di Ceramica: Documenti ed Ipotesi*; CNR: Rome, Italy, 2000; pp. 207–223.
3. Moravetti, A.; Alba, E.; Foddai, L. *La Sardegna Nuragica: Storia e Materiali*; Carlo Delfino: Sassari, Italy, 2014.
4. Minoja, M.; Salis, G.; Usai, L. *L'isola Delle Torri: Giovanni Lilliu e La Sardegna Nuragica: Catalogo Della Mostra*; Carlo Delfino Editore: Cagliari, Italy, 2015; pp. 205–210.
5. Corraine, P. Fiasche del Pellegrino. Problematiche e Prospettive. In La Sardegna e il Mediterraneo: Dall'archeologia alla Società. Studi e Ricerche in Memoria di Ercole Contu, 2020. Available online: https://dumas.uniss.it/it/novita/la-sardegna-e-il-mediterraneo-dallarcheologia-alla-societa-due-giornate-di-studi-memoria-di-ercole-contu (accessed on 26 July 2021).
6. Basoli, P. Nughedu San Nicolo (Sassari). Localita S'Istria. Necropoli ipogeica. *Boll. Archeol.* **1992**, *13–15*, 157.
7. Ialongo, N. Il Santuario Nuragico di Monte Sant'Antonio di Siligo (SS). Studio Analitico dei Complessi Cultuali Della Sardegna Protostorica. Ph.D. Thesis, Archeologia Preistorica, Facoltà di Scienze Umanistiche, Sapienza—Università di Roma, Roma, Italy, 2011.
8. Nocco, C. *Reperti Metallici*; Carlo Delfino Editore: Sassari, Italy, 2015.
9. Usai, E.; Zucca, R. *Nuovi Bronzi Nuragici Dell'Antiquarium Arborense di Oristano: Contributo alle Rotte Mediterranee Della Sardegna*; Carocci Editore: Rome, Italy, 2011; pp. 323–350.
10. Milletti, M. *Cimeli D'Identità: Tra Etruria e Sardegna Nella Prima età del Ferro*; Officina Edizioni: Rome, Italy, 2012.
11. Atzeni, C.; Massidda, L.; Sanna, U. *Le Indagini e i Risultati*; Delfis: Cagliari, Italy, 2011; pp. 136–221.
12. Brunetti, A.; Golosio, B. A new Monte Carlo code for simulation of the effect of irregular surfaces on X-ray spectra. *Spectrochim. Acta Part B At. Spectrosc.* **2014**, *94*, 58–62. [CrossRef]
13. Brunetti, A.; Golosio, B.; Schoonjans, T.; Oliva, P. Use of Monte Carlo simulations for cultural heritage X-ray fluorescence analysis. *Spectrochim. Acta Part B At. Spectrosc.* **2015**, *108*, 15–20. [CrossRef]
14. Angelini, E.; Rosalbino, F.; Grassin, S.; Ingo, G.; De Caro, T. Simulation of corrosion processes of buried archaeological bronze artefacts. In *Corrosion of Metallic Heritage Artefacts*; Woodhead Publishing: Sawston, UK, 2007; pp. 203–218.
15. Schweizer, F. Bronze objects from lake sites: From patina to "biography". In *Ancient and Historic Metals: Conservation and Scientific Research: Proceedings of a Symposium Organized by the J. Paul Getty Museum and the Getty Conservation Institute, November 1991*; Getty Conservation Institute: Marina del Rey, CA, USA, 1994; pp. 33–50. Available online: http://hdl.handle.net/10020/gci_pubs/ancientmetals (accessed on 26 July 2021).
16. Guerra, M.F. *The Study of the Characterisation and Provenance of Coins and Other Metalwork Using XRF, PIXE and Activation Analysis*; Elsevier Science B.V.: Amsterdam, The Netherlands, 2000; pp. 378–416.
17. Figueiredo, E.; Araújo, M.F.; Silva, R.J.; Vilaça, R. Characterisation of a Proto-historic bronze collection by micro-EDXRF. *Nucl. Instrum. Methods Phys. Res. Sect. B Beam Interact. Mater. Atoms* **2013**, *296*, 26–31. [CrossRef]
18. Condamin, J.; Picon, M. The influence of corrosion and diffusion on the percentage of silver in Roman Denarii. *Archaeometry* **1964**, *7*, 98–105. [CrossRef]
19. Sherman, J. The theoretical derivation of fluorescent X-ray intensities from mixtures. *Spectrochim. Acta* **1955**, *7*, 283–306. [CrossRef]
20. Shiraiwa, T.; Fujino, N. Theoretical Calculation of Fluorescent X-Ray Intensities in Fluorescent X-Ray Spectrochemical Analysis. *Jpn. J. Appl. Phys.* **1966**, *5*, 886. [CrossRef]
21. Mantler, M. X-ray fluorescence analysis of multiple-layer films. *Anal. Chim. Acta* **1986**, *188*, 25–35. [CrossRef]
22. De Boer, D. Calculation of X-ray fluorescence intensities from bulk and multilayer samples. *X-Ray Spectrom.* **1990**, *19*, 145–154. [CrossRef]
23. Bottigli, U.; Brunetti, A.; Golosio, B.; Oliva, P.; Stumbo, S.; Vincze, L.; Randaccio, P.; Bleuet, P.; Simionovici, A.; Somogyi, A. Voxel-based Monte Carlo simulation of X-ray imaging and spectroscopy experiments. *Spectrochim. Acta Part B At. Spectrosc.* **2004**, *59*, 1747–1754. [CrossRef]
24. Golosio, B.; Schoonjans, T.; Brunetti, A.; Oliva, P.; Masala, G.L. Monte Carlo simulation of X-ray imaging and spectroscopy experiments using quadric geometry and variance reduction techniques. *Comput. Phys. Commun.* **2014**, *185*, 1044–1052. [CrossRef]
25. Schoonjans, T.; Brunetti, A.; Golosio, B.; del Rio, M.S.; Solé, V.A.; Ferrero, C.; Vincze, L. The xraylib library for X-ray—Matter interactions. Recent developments. *Spectrochim. Acta Part B At. Spectrosc.* **2011**, *66*, 776–784. [CrossRef]
26. Nørgaard, H.W. Portable XRF on prehistoric bronze artefacts: Limitations and use for the detection of Bronze Age metal workshops. *Open Archaeol.* **2017**, *3*, 101–122. [CrossRef]
27. Ingo, G.; De Caro, T.; Riccucci, C.; Angelini, E.; Grassini, S.; Balbi, S.; Bernardini, P.; Salvi, D.; Bousselmi, L.; Cilingiroglu, A.; et al. Large scale investigation of chemical composition, structure and corrosion mechanism of bronze archeological artefacts from Mediterranean basin. *Appl. Phys. A* **2006**, *83*, 513–520. [CrossRef]
28. Chiriu, D.; Ricci, P.; Cappellini, G. Raman characterization of XIV–XVI centuries Sardinian documents: Inks, papers and parchments. *Vib. Spectrosc.* **2017**, *92*, 70–81. [CrossRef]
29. Buzgar, N.; Apopei, A.I. The Raman study of certain carbonates. *Anal. Şt. Univ. Al. I. Cuza Iaşi Geol.* **2009**, *2*, 97–112.

30. Colomban, P.; Tournié, A.; Maucuer, M.; Meynard, P. On-site Raman and XRF analysis of Japanese/Chinese bronze/brass patina–the search for specific Raman signatures. *J. Raman Spectrosc.* **2012**, *43*, 799–808. [CrossRef]
31. Kosec, T.; Ropret, P.; Legat, A. Raman investigation of artificial patinas on recent bronze—Part II: Urban rain exposure. *J. Raman Spectrosc.* **2012**, *43*, 1587–1595. [CrossRef]
32. Chan, H.Y.H.; Takoudis, C.G.; Weaver, M.J. Oxide film formation and oxygen adsorption on copper in aqueous media as probed by surface-enhanced Raman spectroscopy. *J. Phys. Chem. B* **1999**, *103*, 357–365. [CrossRef]
33. Ospitali, F.; Chiavari, C.; Martini, C.; Bernardi, E.; Passarini, F.; Robbiola, L. The characterization of Sn-based corrosion products in ancient bronzes: A Raman approach. *J. Raman Spectrosc.* **2012**, *43*, 1596–1603. [CrossRef]
34. McCann, L.I.; Trentelman, K.; Possley, T.; Golding, B. Corrosion of ancient Chinese bronze money trees studied by Raman microscopy. *J. Raman Spectrosc.* **1999**, *30*, 121–132. [CrossRef]
35. Robbiola, L.; Blengino, J.M.; Fiaud, C. Morphology and mechanisms of formation of natural patinas on archaeological Cu–Sn alloys. *Corros. Sci.* **1998**, *40*, 2083–2111. [CrossRef]
36. Hayez, V.; Costa, V.; Guillaume, J.; Terryn, H.; Hubin, A. Micro Raman spectroscopy used for the study of corrosion products on copper alloys: Study of the chemical composition of artificial patinas used for restoration purposes. *Analyst* **2005**, *130*, 550–556. [CrossRef] [PubMed]
37. Chu, P.K.; Li, L. Characterization of amorphous and nanocrystalline carbon films. *Mater. Chem. Phys.* **2006**, *96*, 253–277. [CrossRef]
38. Fang, J.L.; McDonnell, G. The colour of copper alloys. *Hist. Metall.* **2011**, *45*, 52.